IEEE Access
Multidisciplinary | Rapid Review | Open Access Journal

Received November 25, 2019, accepted December 13, 2019, date of publication December 17, 2019,
date of current version December 26, 2019.

Digital Object Identifier 10.1109/ACCESS.2019.2960372

Terahertz Band Propagation Characteristics of Coupling Multiconductor Transmission Lines in Multilayer Media

XINYU WANG, DAN ZHANG, (Member, IEEE), AND JING ZHU
College of Information Science and Technology, Nanjing Forestry University, Nanjing 210037, China

Corresponding author: Dan Zhang (zhangdan@njfu.edu.cn)

This work was supported in part by the Postgraduate Research and Practice Innovation Program of Jiangsu Province and in part by the High-level Talents Project of Nanjing Forestry University.

ABSTRACT The study on terahertz radiators will not only boost the development of theoretical research, but also raise severe challenges to solid-state electronics and circuit technology. In the present paper, the transmission characteristics of microstrip-slot coupling structures are primarily studied in 1-3THz band. Based on the single-layer dielectric structure, a double-layer dielectric microstrip-slot coupling structure with air as one layer is presented. It is reported that adding air layer based on the single-layer structure helps reduce the loss. Besides, given the factors of Engineering processing, the structure of three-layer media is also proposed; it is found that the structure of three-layer media still has exhibits transmission loss when the engineering realization is satisfied. However, this study suggests that the loss of the three-layer structure is higher than that of the two-layer structure, whereas the effect is better than that of the single-layer structure.

INDEX TERMS Terahertz, multilayer structure, transmission characteristics, odd mode, even mode.

I. INTRODUCTION

Terahertz radiation refers to the electromagnetic radiation of 0.1-10THz. From the frequency perspective, it is between radio wave and light wave, as well as between millimeter wave and infrared line. From the energy perspective, the infrared and microwave technology on both sides of terahertz band has been highly mature in the electromagnetic spectrum between electron and photon, whereas the terahertz technology is almost empty. This is because in this frequency band, it is not entirely suitable for optical theory to deal with, nor is it entirely applicable for microwave theory to study [1].

The advantages of terahertz wave lead to high research implication in many fields. In communication, terahertz wave exhibits higher frequency than millimeter wave terahertz wave, so terahertz wave can provide wider bandwidth and transmit more information when employed in communication [1]–[3]. As stimulated by the further maturity of terahertz technology, the application of terahertz technology in high-speed and short-range wireless communication has been achieved. In the aspect of security detection, due to several characteristics of terahertz wave, terahertz wave can penetrate clothing to find dangerous goods and will not jeopardize people and goods. In the medical field, terahertz wave is safer and more practical than X-ray as it can image the human body with relatively high accuracy without adverse effects [4], [5]. In the military field, terahertz wave is hard to leak for its good direction and narrow beam in the transmission process, so it exhibits a promising application in short-range tactical communication [6]. In the meantime, terahertz transmission in the atmosphere will have a greater attenuation, and the terahertz wave is hard to detect in the distance, so it can be used. Moreover, radar has better resolution in terahertz band and can detect target more accurately [7].

Though terahertz wave exhibits numerous unique properties compared with other frequency bands, it also shows some limitations [8]. First is the limitation of technical means. Although terahertz technology has achieved great progress in the past decades, the research field of terahertz frequency band has been insufficiently mature thus far, and there are many places worth studying in depth [9]. Second, terahertz radiation has some physical limitations. For conductive objects, terahertz cannot penetrate, so metals and other materials cannot leverage terahertz wave for perspective study [10]–[17]. Besides, since the gas in the air absorbs

The associate editor coordinating the review of this manuscript and approving it for publication was Guan Gui.

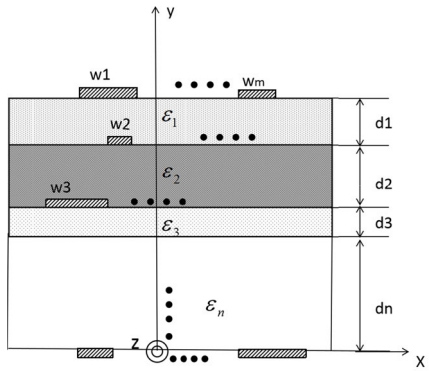

FIGURE 1. Cross section of dielectric multilayered coupled multi-conductor transmission lines.

terahertz energy, terahertz wave propagation in the air displays a significant loss and cannot be transmitted over long distances [18], [19].

The advantages of terahertz wave should make it of high research implication in numerous fields [20]–[24]. In communication, terahertz wave exhibits higher frequency than millimeter wave terahertz wave, so terahertz wave can provide wider bandwidth and transmit more information when employed in communication [25]–[27].

To meet the need of planar integration of terahertz systems, some planar transmission lines (e.g., microstrip [28], stripline [29], [30], slot-line [31] and coplanar wave-guide [32]) have been proposed to transmit terahertz waves [14]. To keep abreast with advancement of wireless communication systems, transmission structures are progressively pursuing miniaturization in design [33], [34]. Since multilayer structure can fully exploit the upper and lower sides of the dielectric substrate to reduce size, a growing number of people use multilayer structure in design, as shown in Fig. 1. Microstrip line and slot line are the two commonest planar transmission lines [31]. Microstrip line displays the advantages of small size and easy integration. Slot line can be adopted in high impedance line, series short line and short circuit [35]. With their combination, a microstrip-slot coupling structure is formed [31], exhibiting more degrees of freedom in the design process. If the required circuits consisting of microstrip lines and slot lines are made on both sides of the identical dielectric substrate, the coupling between them can be leveraged to construct components (e.g., filters and directional couplers) [36]–[38]. Accordingly, in most cases, the microstrip-slot coupling structure is employed to transmit signals between the upper and lower sides of the dielectric substrate. The integrated design based on microwave is freely applied in these structures. From the perspective of reducing size and improving transmission performance, this paper proposes adding air box to establish two novel structures. The one is the suspended lower air microstrip-slot coupled structure, and the other is the upper air microstrip-slot coupled structure. In the present paper, the transmission characteristics of microstrip-slot coupled structures are studied. Consider coupled M transmission conductors situated in a N -layered dielectric substrate over a ground plane of perfect conductor [39]. The strips of widths $w_v (v = 1, 2, \ldots, M)$ are assumed to be perfect conductors of t thickness. The center of the v-th strip is located at x $=x_v$. The thickness and relative dielectric constant of the n-th layer are h_n and $\varepsilon_n (n = 1, 2, \ldots, N)$, respectively.

The coupled-mode equations are formulated using the generalized reciprocity relation [40]. The electromagnetic fields and currents of the coupled lines in Fig. A are approximated as follows:

$$\mathbf{E}\,(\mathrm{x}, \mathrm{y}, \mathrm{z}) = \sum_{v=1}^{M} a_v\,(z)\,\boldsymbol{e}_v\,(x, y) \tag{1}$$

$$\mathbf{H}\,(\mathrm{x}, \mathrm{y}, \mathrm{z}) = \sum_{v=1}^{M} a_v(z)\boldsymbol{h}_v(x, y) \tag{2}$$

$$\mathbf{J}\,(\mathrm{x}, \mathrm{y}, \mathrm{z}) = \sum_{v=1}^{M} a_v\,(z)\boldsymbol{j}_v(x, y) \tag{3}$$

where $a_v\,(z)$ are unknown amplitude functions and $\boldsymbol{e}_v(x, y)$, $\boldsymbol{h}_v(x, y)$ and $\boldsymbol{j}_v(x, y)$ are the eigenmode functions for the fields and currents propagating in the +z direction along M transmission conductors. The eigenmode fields and currents propagating in the −z direction in the respective transmission conductors are expressed as follow:

$$\boldsymbol{E}'_v = \left[\boldsymbol{e}_{v,t}\,(x, y) - \hat{\boldsymbol{z}} e_{v,z}\,(x, y)\right] \exp\left(n\beta_v z\right) \tag{4}$$

$$\boldsymbol{H}'_v = \left[-\boldsymbol{h}_{v,t}\,(x, y) + \hat{\boldsymbol{z}} h_{v,z}\,(x, y)\right] \exp\left(n\beta_v z\right) \tag{5}$$

$$\boldsymbol{J}'_v = \left[\hat{\boldsymbol{X}} j_{v,t}\,(x, y) - \hat{\boldsymbol{z}} j_{v,z}\,(x, y)\right] \exp\left(n\beta_v z\right) \tag{6}$$

where β_v is the propagation constant of the isolated v-th transmission conductors, and the subscripts t, x, and z denote the transverse, x and z components of the indicated vectors, respectively. Substituting Eqs. (1) – (3) and Eqs. (4) – (6) for each of transmission conductors into the generalized reciprocity relation, the coupled-differential equations governing the evolutions of modal amplitudes $a_v(z)$ are derived as follows:

$$\frac{d}{dz}\boldsymbol{a} = -i\,[\boldsymbol{C}]\,\boldsymbol{a} \tag{7}$$

And transmission conductors "v" and "μ" located in the original dielectric layers as shown in Fig. 1

$$\mathbf{a} = [a_1\,(\mathrm{z})\,a_2\,(\mathrm{z})\,a_3\,(\mathrm{z})]^T \tag{8}$$

$$[\mathrm{C}] = [M]^{-1}\,[K] \tag{9}$$

$$K_{v\mu} = \beta_v M_{v\mu} + Q_{v\mu} \tag{10}$$

$$M_{v\mu} = \frac{1}{2}\left(N_{v\mu} + N_{\mu v}\right) \tag{11}$$

$$N_{v\mu} = \frac{1}{2}\int_S \left[\boldsymbol{e}_v(x, y) \times \boldsymbol{h}_\mu(x, y)\right] \cdot \hat{\boldsymbol{z}}\,dxdy \tag{12}$$

$$Q_{v\mu} = -\frac{n}{4}\int_{l_\mu} \left[e_{v,x}\,(x, y)\,j_{\mu,x}\,(x, y) - e_{v,z}\,(x, y)\,j_{\mu,z}\,(x, y)\right] dxdy \tag{13}$$

where S represents the cross-sectional area of the structure, l_μ denotes the cross-sectional contour of the μ-th line, and the eigenmode fields and currents in the isolated lines are normalized so that $N_{vv} = 1$. Note that $Q_{vv} = 0$ since $e_{v,x}(x, y) = e_{v,z}(x, y) = 0$ on the surface of the v-th line. Equation (7) is the coupled-mode equations which play the same role as the transmission line equations in the quasi-static approach. The solutions determine the propagation constant β_m of the coupled mode m and the modal amplitude a_{vm} of the current on the v-th line [39].

Although various numerical techniques have been developed for the rigorous analysis of coupled lines, those direct solution methods become much more involved and are very time consuming computationally when the number of lines increases. The methods based on the full-wave analysis proposed in this paper effectively improves the accuracy and reduces the calculation.

The problem of coupled transmission conductors was reduced to that of isolated transmission conductors. When the eigenmode fields and currents for the isolated N lines are obtained, the coupling coefficients $K_{v\mu}, N_{v\mu}$, and $Q_{v\mu}$ governing the interaction between the v -th and μ-th lines are easily calculated by the overlap integrals given by Eqs. (12) and (13). These integrals can be efficiently performed [40], [41] in the spectral domain by using the Galerkin's moment method solutions for the conventional single transmission conductor. The details of this numerical method have been well documented in the open literature [42]. The reciprocity relation [40], [41] between the eigenmode fields of the isolated v-th and μ-th lines leads to the identity

$$\beta_v M_{v\mu} + K_{v\mu} = \beta_v M_{\mu v} + K_{\mu v} \tag{14}$$

This relation reduces the calculation of the coupling matrix [C] in Eq. (7).

To verify the feasibility of our method, the propagation characteristics of THz pulses on microstrip-lines are studied and compared by referencing [21] as the baseline. The attenuation constant and the effective index of refraction of microstrip line (MSL) and coplanar strip lines (CPS) are plotted as functions of frequency in Fig.2-3. In Fig. 3, the squares, diamonds, and circles represent the sapphire, quartz, and polymer substrates, respectively. The dotted-dash, dash, and solid lines represent the sapphire, quartz, and polymer substrates, respectively. Our results are consistent with the predictions based on the analytical formula used in microwave regime [21], [43].

II. DOUBLE-LAYER DIELECTRIC MICROSTRIP-SLOT COUPLING STRUCTURE

In this paper, based on the single-layer dielectric microstrip-slot coupling structure, a double-layer dielectric microstrip-slot coupling structure is proposed, in which one layer dielectric is air [1], [43]. Multilayer structure is a novel structure in the terahertz wave band [1].

In the double-layer microstrip-slot coupling structure with air in the lower layer, the overall thickness of the dielectric

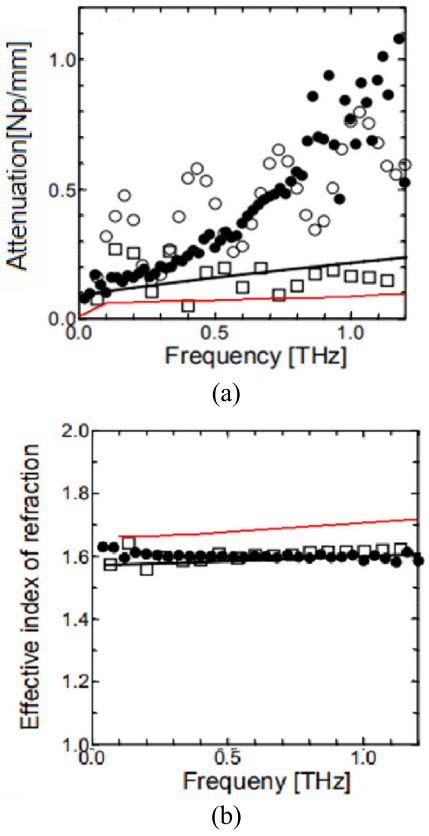

FIGURE 2. The (a) attenuation constant and (b) effective index-of refraction associated with the propagation of the THz pulses along the MSL are presented. The solid circles and open squares represent the experimental and FDTD results, respectively. The black solid line and the open circles in (a) refer to the values estimated using the analytical expressions used in the microwave regime with the measured conductance of the metal line and the tangent of the polyimide film, respectively. The black solid lines in (b) is a prediction based on a model in microwave regime. The red lines are our results.

layer is h $= 20 \times 10^{-3}$mm as a fixed value, and the material of the microstrip and slot is copper with the thickness t $= 0.2 \times 10^{-3}$mm, as shown in Fig. 4. The thickness of the metal can be ignored compared with that of the medium, so the effect of the thickness of the metal on the transmission characteristics is not discussed here. In practice, metals and dielectrics should be lossy; thus, in the analysis, the conductor strip and the floor are set as lossy copper, the dielectrics are set as dielectric constant, and the loss angle is tangent nonmagnetic material.

Note that dielectric loss tangent is negligible in terahertz band. For the high frequency, small tangent of loss angle can also cause larger dielectric loss. Given this, even if the tangent of loss angle is very small, the tangent of loss angle cannot be set to 0. The width of the upper microstrip is w $= 20 \times 10^{-3}$mm, unchanged. The width of the lower slot is s $= 20 \times 10^{-3}$mm without change. The lower layer refers to an air layer, and the upper layer represents a dielectric substrate with a thickness of d1 and a dielectric constant of ε_1.

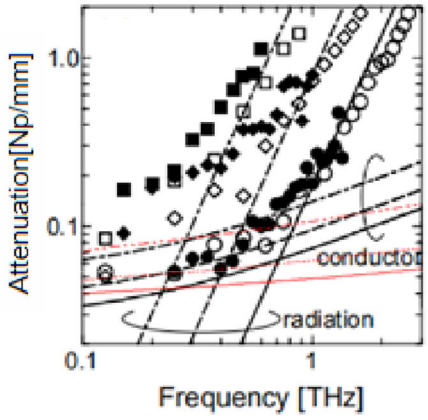

(a)

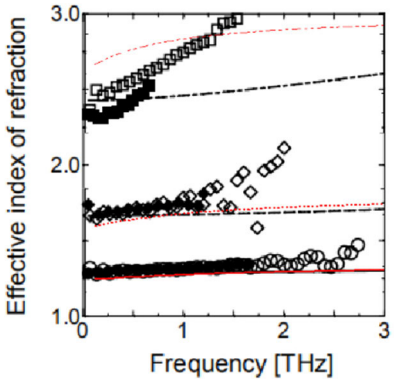

(b)

FIGURE 3. The (a) attenuation constant and (b) effective index-of-refraction associated with the propagation of THz pulses along the CPS are presented. The solid and open symbols denote the experimental and the FDTD results, respectively. The black lines are the predictions based on an analytical formula adopted in the microwave regime. The red lines represent our results.

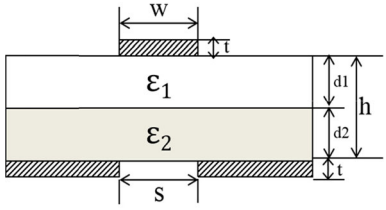

FIGURE 4. Cross section of doubled-layer dielectric microstrip-slot coupling structure.

The double-layer microstrip-slot coupling structure with air in the upper layer indicates that the upper layer is an air layer, and the lower layer refers to a dielectric substrate with a thickness of d2 and a dielectric constant of ε_2. Other parameters comply with the double-layer microstrip-slot coupling structure with air in the upper layer.

The effective dielectric constant can be approximately expressed as Eqs. (15)

$$\varepsilon_r = \frac{h}{d_1/\varepsilon_1 + d_2/\varepsilon_2} \tag{15}$$

The dielectric constant of the dielectric plate is greater than that of air. The increase in the thickness of the dielectric plate is the decrease in the height of the air layer. According to the Eqs. (15), it can be obtained that the effective dielectric constant increases with the increase in the thickness of the dielectric plate.

The relationship between loss and effective dielectric constant is expresses as Eqs. (16)

$$\alpha \propto \mathrm{f} \cdot \tan\delta\sqrt{\varepsilon_r} \tag{16}$$

Therefore, with the increase of the height of the dielectric plate, the loss will increase correspondingly, and the corresponding attenuation will also increase accordingly.

During the simulation process, the premise is that the total thickness of the dielectric substrate remains unchanged. The dielectric constant of the two types of dielectric substrates is a variable, and the dielectric constant is set to 2, 4, and 6, respectively. The transmission characteristics are observed. On the other hand, regulating the thickness of the dielectric substrate makes the composition ratio of the air layer to the substrate a variable, whereas it does not change the dielectric constant and observe the variation of transmission characteristics.

A. THE DOUBLE-LAYER MICROSTRIP-SLOT COUPLING STRUCTURE WITH AIR IN THE LOWER LAYER

When the dielectric constant under odd mode excitation is 2, 4, and 6, the effective dielectric constant varies with the thickness of the dielectric substrate. First, the dielectric constant of the dielectric substrate is one of the factors affecting the effective dielectric constant. As indicated by solid line in Fig. 5, the larger the dielectric constant of the substrate, the larger the effective dielectric constant will be under odd mode excitation. On the other hand, the thickness of dielectric plate is also one of the influencing factors. The larger the thickness, the bigger the effective dielectric constant will be.

In the meantime, the change curve of attenuation constant is also measured when the dielectric constant under odd mode excitation is 2, 4, and 6. As shown by dotted line in Fig. 5, with the rise in the thickness of the dielectric substrate, the attenuation curve will change, the effective dielectric constant will increase, and the attenuation constant will be up-regulated. Accordingly, consistent with the above description of the effective dielectric constant, the larger the dielectric constant, the more significant the attenuation, the higher the frequency, and the more noticeable the difference will be. However, at the thickness of the dielectric substrate of 16um, the attenuation is inclined to decrease, i.e., under the excitation of odd modes, the attenuation of the suspended microstrip line is also reduced, so the total attenuation will be mitigated [32], [44], [45].

The blue solid line, the green solid line, the red solid line and the black solid line in Fig. 5, 6, 9, 10 represent the different measurement conditions of dielectric thickness d1 of 16um$\times 10^{-3}$mm, 12$\times 10^{-3}$mm, 8$\times 10^{-3}$mm and 4$\times 10^{-3}$mm, respectively. The blue dotted line, the green

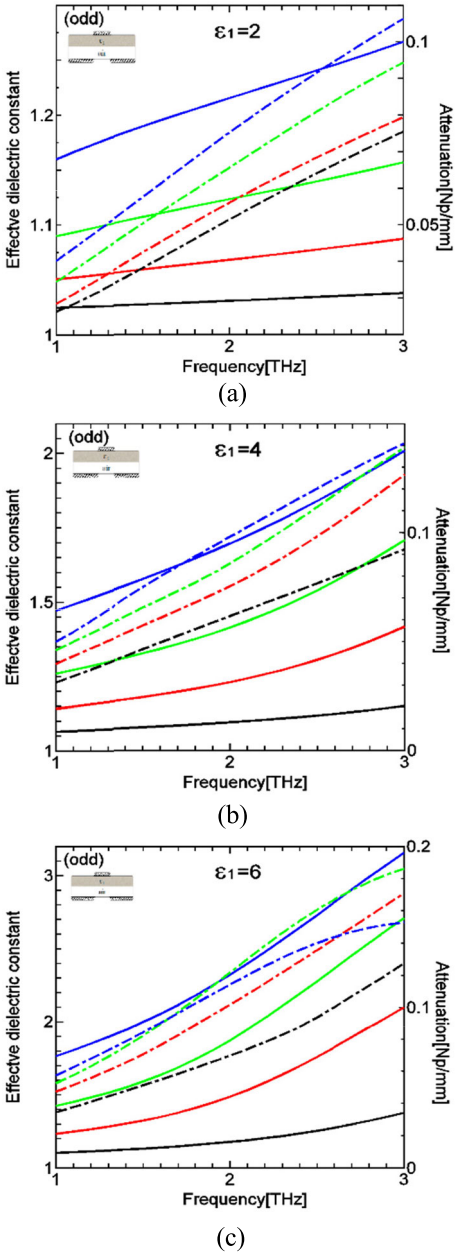

FIGURE 5. Under odd mode excitation, the effective dielectric constant versus frequency curves when ε_1 is (a) 2, (b) 4, and (c) 6. Solid lines represent effective dielectric constant, dotted lines represent attenuation.

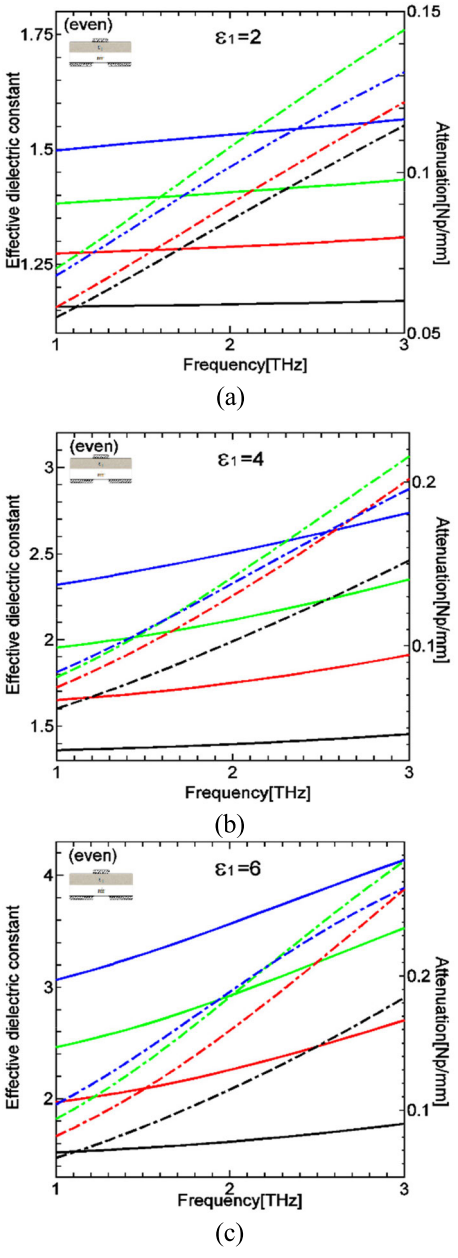

FIGURE 6. Under even mode excitation, the effective dielectric constant versus frequency curves when ε_1 is (a) 2, (b) 4, and (c) 6. Solid lines represent effective dielectric constant, dotted lines represent attenuation.

dotted line, the red dotted line and the black dotted line in Fig. 5, 6, 9, 10 indicate the different measurement conditions of dielectric thickness d1 of $16\text{um}\times10^{-3}$mm, 12×10^{-3}mm, 8×10^{-3}mm and 4×10^{-3}mm, respectively.

When the dielectric constant ε_1 is 2, 4, and 6, under even mode excitation, the change curve of effective dielectric constant is presented by solid line in Fig. 6. The varying trend of dielectric constant is identical to that under odd mode excitation.

When the dielectric constant ε_1 is 2, 4, and 6, under even mode excitation, the attenuation curve is presented by dotted line in Fig. 6. With the rise in the thickness of the dielectric substrate, the attenuation varies more significantly. Besides, under the identical dielectric constant, the attenuation of the structure with the dielectric substrate thickness of 12×10^{-3}mm in high frequency band is larger than that of other structures, and the reason for change belongs to the variation of radiation loss.

In the double-layer microstrip-slot coupling structure with air in the lower layer, it is found that the higher the dielectric constant of the substrate at 3THz, the higher the effective dielectric constant and attenuation will be in both odd and even modes. Moreover, under the identical condition, the effective dielectric constant and attenuation

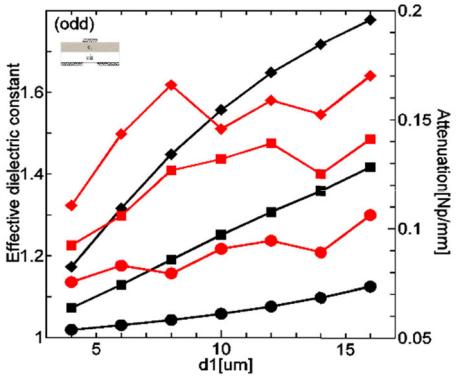

FIGURE 7. Curve of effective dielectric constant and attenuation with thickness of dielectric plate in odd mode. Black lines represent effective dielectric constant, red lines represent attenuation.

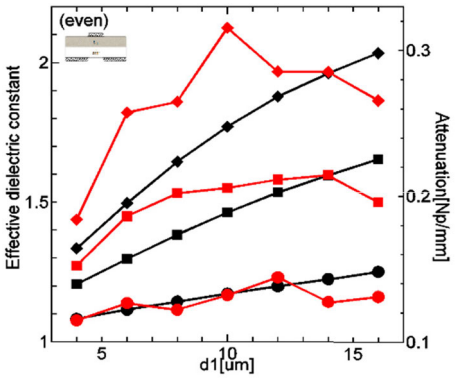

FIGURE 8. Curve of effective dielectric constant and attenuation with thickness of dielectric plate in even mode. Black lines represent effective dielectric constant, red lines represent attenuation.

will be larger in even mode than in odd mode. Nevertheless, Fig. 5 and 6 suggest that with the rise in dielectric thickness and dielectric constant, the attenuation of the structure of the dielectrics is obviously different, and the attenuation decreases with the rise in thickness and dielectric constant.

In the present paper, the relation curves of effective dielectric constant and attenuation constant with the thickness of dielectric substrate at 3THz are also made. As presented by black lines in Fig. 7-8, the effective dielectric constant increases with the rise in the thickness of the dielectric plate whether excited by odd or even modes. Attenuation constant is presented by red lines in Fig. 7-8. Under odd mode excitation, when the dielectric constant of the medium is 2 or 4, the attenuation constant is up-regulated with the rise in the thickness. However, it is suggested that with the rise in the dielectric constant, the amplitude of attenuation increase decreases. When the dielectric constant is 6, the attenuation constant obviously increases first and then decreases. Under even mode excitation, the curve changes more prominent, and the attenuation constant increases first and then decreases. A solid black line with circle represents the effective dielectric constant when $\varepsilon_1 = 2$; a solid black line with square represents the effective dielectric constant when $\varepsilon_1 = 4$; a

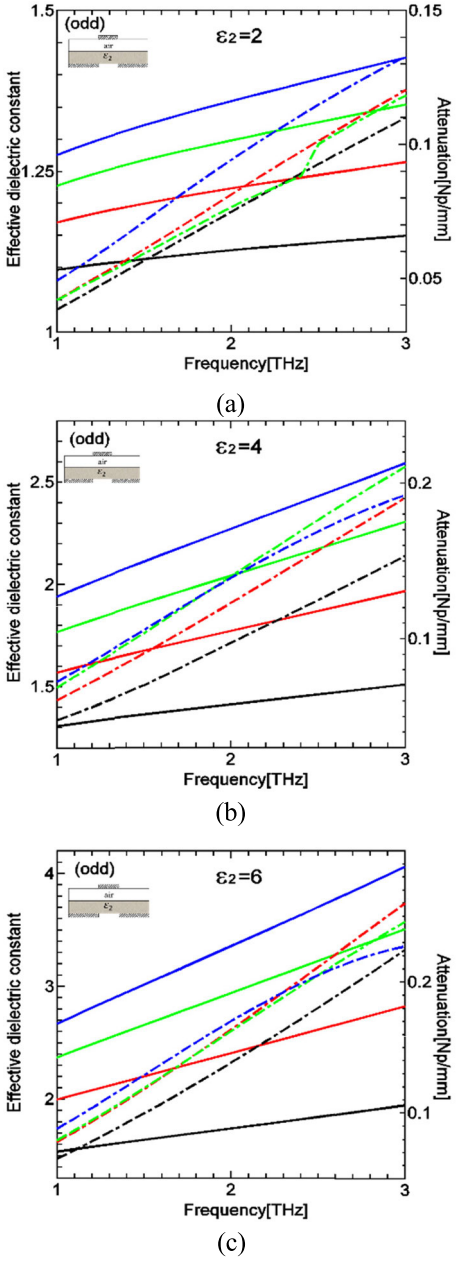

FIGURE 9. Under odd mode excitation, the effective dielectric constant versus frequency curves when ε_2 is (a) 2, (b) 4, (c) 6, Solid lines represent effective dielectric constant, dotted lines represent attenuation.

solid black line with diamond denotes the effective dielectric constant when $\varepsilon_1 = 6$; a solid red line with circle indicates the attenuation when $\varepsilon_1 = 2$; a solid red line with square shows the attenuation when $\varepsilon_1 = 4$; a solid red line with diamond represents the attenuation when $\varepsilon_1 = 6$, as shown in Fig. 7,8,9,11,12, respectively.

Unexpected attenuation is discussed here [27], [28], and [37]. The attenuation in this paper includes dielectric loss, conductor loss and radiation loss. When the thickness and dielectric constant of the dielectric substrate are rising, the conductor loss and dielectric loss will increase, while the radiation loss will be lowered. When the thickness rises

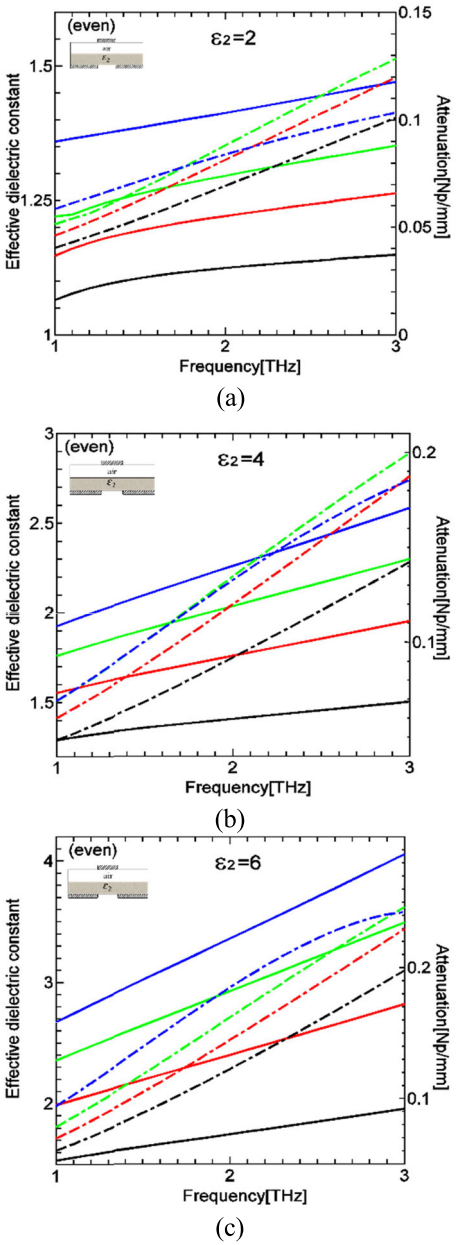

FIGURE 10. Under even mode excitation, the effective dielectric constant versus frequency curves when ε_1 is (a) 2, (b) 4, (c) 6. Solid lines represent effective dielectric constant, dotted lines represent attenuation.

to 16×10^{-3}mm, the radiation loss will decrease more significantly than the previous attenuation, and then the total attenuation will be reduced.

B. THE DOUBLE-LAYER MICROSTRIP-SLOT COUPLING STRUCTURE WITH AIR IN THE UPPER LAYER

In the subsequent cases, the variation of effective dielectric constant and attenuation constant under odd mode and even mode is also measured by varying the position of air layer and dielectric substrate. Under odd mode excitation, when the dielectric constant of the substrate is 2, 4, and 6, the change curve of effective dielectric constant with the thickness of the substrate is presented by solid line (Fig. 9). The larger the dielectric constant of the substrate, the higher the effective dielectric constant, and the higher the thickness of the substrate, the larger the effective dielectric constant will be.

When the dielectric constant is 2, 4, and 6, under odd mode excitation, the curve of attenuation constant varies with the thickness of dielectric substrate as shown by dotted line in Fig. 9. Obviously, attenuation increases with the rise in dielectric constant of substrate; whereas under the corresponding conditions, the effect is not obvious. Likewise, the thickness of the dielectric substrate has an effect on the attenuation, but after reaching a certain thickness, the attenuation gradually decreases with the rise in the dielectric constant and the thickness of the dielectric substrate.

When the dielectric constant is 2, 4, and 6, under the even mode excitation, the effective dielectric constant varies with the thickness of the dielectric substrate, as presented by solid line in Fig.10. The effective dielectric constant varies more obviously when the dielectric constant of the dielectric substrate is up-regulated with the transmission of the dielectric substrate. The effective dielectric constant also increases with the rise in the dielectric constant of the dielectric substrate. The larger the thickness of the dielectric substrate, the bigger the dielectric constant will be, and the variation will be more obvious.

When the dielectric constant is 2, 4, and 6, under even mode excitation, the attenuation curve varies with the thickness of the dielectric substrate. According to the dotted line in Fig. 10, the larger the dielectric constant of the substrate, the larger the attenuation constant will be. In the 1THz to 3THz bands, it is found that there is also a boundary point where the attenuation is reduced when the radiation loss decreases.

Besides, for the structure of upper air, the variation curves of effective dielectric constant and attenuation constant with the thickness of the dielectric plate at 3THz are also analyzed. As shown in Fig. 11, the effective dielectric constant increases with the rise in the thickness regardless of the odd mode or even mode excitation. For loss, as shown in Fig. 12, first, under odd mode excitation, when the dielectric constant is 2, the attenuation constant will increase with the rise in thickness. When the dielectric constant is 4, 6, the attenuation constant will increase first and then decrease. Under even-mode excitation, the three dielectric constants all show the identical condition. It is suggested that with the rise in the thickness of the dielectric substrate, the radiation loss will be lowered. When the medium is small, the binding effect on the field will be not robust, and the reduction of radiation loss will be smaller than the rise in conductor loss and medium loss. When the thickness is larger, the medium has a strong binding effect on the field. When the thickness rises to a certain extent, the decrease in radiation loss is larger than the rise in conductor loss and medium loss.

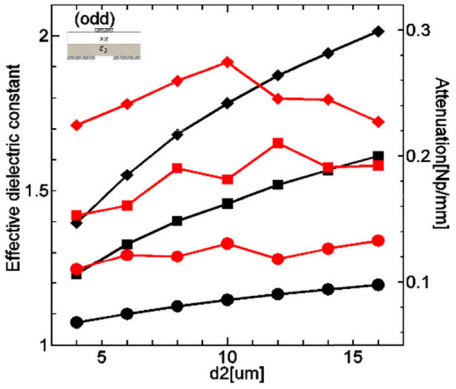

FIGURE 11. Curve of effective dielectric constant and attenuation with thickness of dielectric plate in odd mode. Black lines represent effective dielectric constant, red lines represent attenuation.

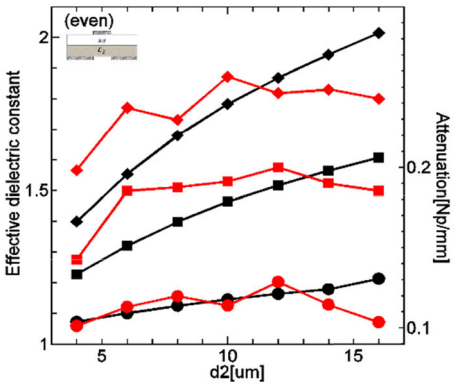

FIGURE 12. Curve of effective dielectric constant and attenuation with thickness of dielectric plate in even mode. Black lines represent effective dielectric constant, red lines represent attenuation.

III. THE THREE-LAYER MICROSTRIP-SLOT COUPLING STRUCTURE WITH AIR IN THE MIDDLE LAYER

Compared with the two-layer structure, and the size of the slot spacing remain unchanged. To explore the transmission characteristics of the three-layer microstrip-slot coupling structure which is shown as Fig. 13, only the dielectric constant and the structure of the transmission dielectric plate are changed.

The curves of effective dielectric constant, under odd mode excitation, are shown by solid line in Fig. 14. When the dielectric constant of the third layer is 2, and the thickness of the third layer is 4×10^{-3}mm, the dielectric constant of the first layer substrate will be 2, 4, and 6, respectively. When the thickness of the first layer dielectric is 4×10^{-3}mm, 8×10^{-3}mm, 12×10^{-3}mm and 14×10^{-3}mm, the curves of effective dielectric constant will vary with the dielectric constant of the first layer, suggesting that the dielectric constant of the first layer varies with the dielectric constant of the first layer. The effective dielectric constant increases with the rise in thickness. Likewise, as the solid lines shown in Fig. 14, the effective dielectric constant increases with the rise in thickness.

Under odd mode excitation, the attenuation constant of three-layer dielectric structure changes as shown by dotted line in Fig. 14. It is reported that the curve changes almost the same, whereas when the third layer dielectric is a definite value, the thicker the first layer dielectric layer, the more

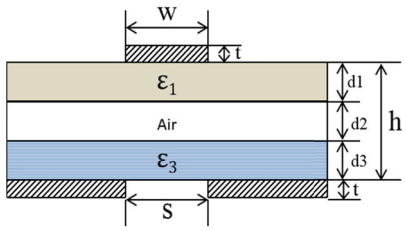

FIGURE 13. Cross section of the three-layer microstrip-slot coupling structure.

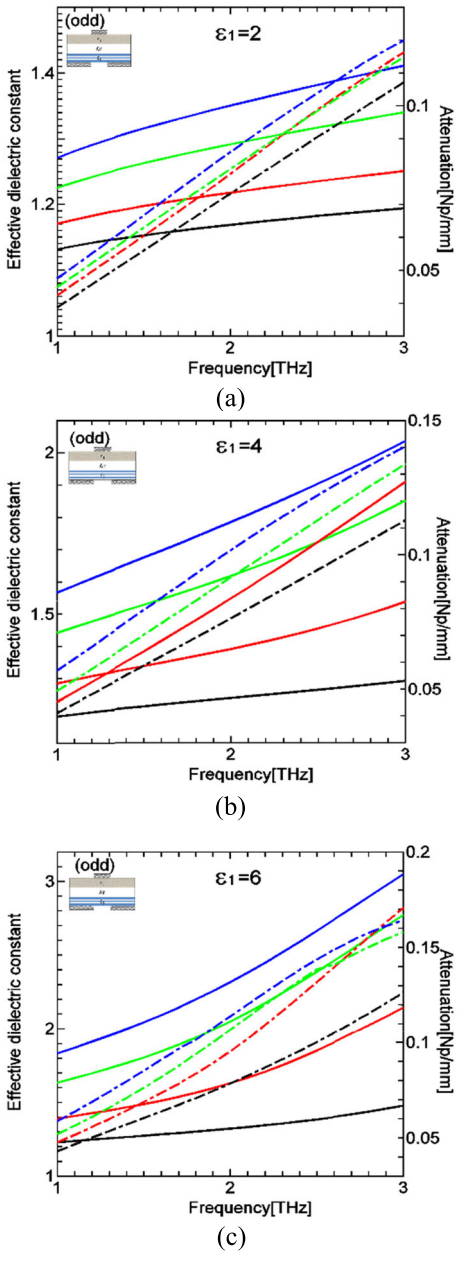

FIGURE 14. Under odd mode excitation, the effective dielectric constant versus frequency curves when ε_1 is (a) 2, (b) 4, (c) 6. Solid lines represent effective dielectric constant, dotted lines represent attenuation.

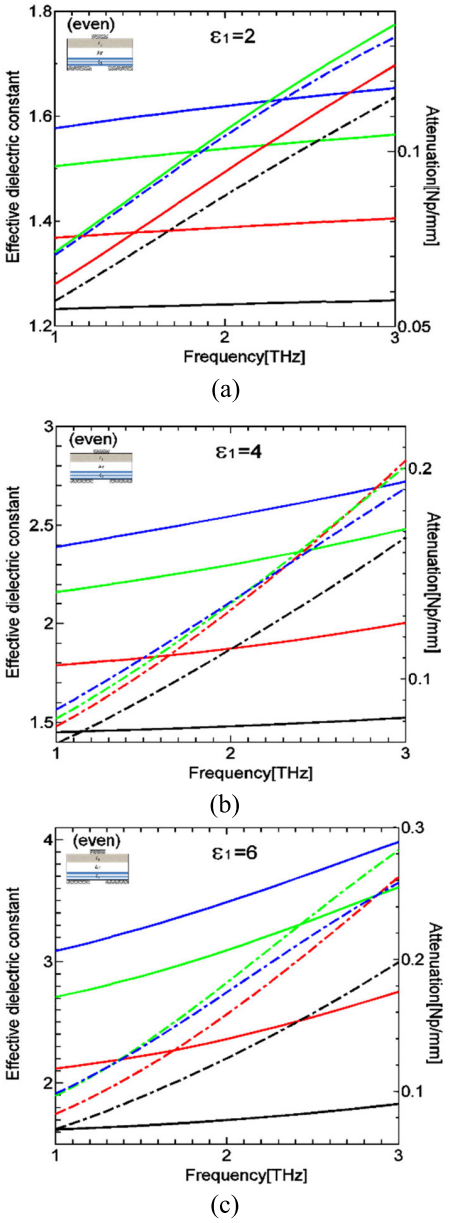

FIGURE 15. Under even mode excitation, the effective dielectric constant versus frequency curves when ε_1 is (a) 2, (b) 4, (c) 6. Solid lines represent effective dielectric constant, dotted lines represent attenuation.

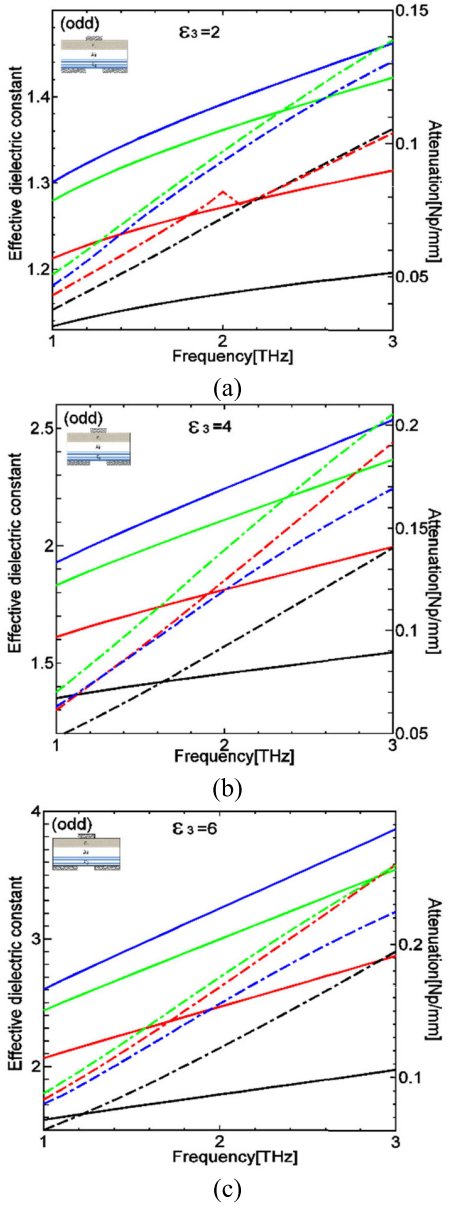

FIGURE 16. Under odd mode excitation, the effective dielectric constant versus frequency curves when ε_3 is (a) 2, (b) 4, (c) 6. Solid lines represent effective dielectric constant, dotted lines represent attenuation.

significant the attenuation will be, while the larger the dielectric constant, the more significant the attenuation will be, but after 2.5THz, there will be a contrast and the attenuation constant will decrease. It is consistent with the double-layer structure.

The blue solid line, the green solid line, the red solid line and the black solid line in Fig. 14-17 denote the different measurement conditions of dielectric thickness of 14×10^{-3}mm, 12×10^{-3}mm, 8×10^{-3}mm and 4×10^{-3}mm, respectively. The blue dotted line, the green dotted line, the red dotted line and the black dotted line in Fig. 14-17 represent the different measurement conditions of dielectric thickness of 14×10^{-3}mm, 12×10^{-3}mm, 8×10^{-3}mm and 4×10^{-3}mm, respectively.

Under the even mode excitation, the total height, the thickness of the third layer and the material of the third layer are not changed as well. We only change the material of the first layer, the dielectric constant is 2, 4, and 6, the thickness of the first layer and the thickness of the air layer caused by the change of the substrate. The effective dielectric constant rises with the odd mode excitation.

The attenuation curve under even mode excitation is shown in Fig. 15. With the rise in dielectric constant, the attenuation will increase correspondingly. However, it is found that in the identical medium, the thicker first layer substrate will not lead to the bigger attenuation. Moreover, the bigger the dielectric constant of the first layer, the more obvious the contrast will appear. Furthermore, with the rise in thickness, the

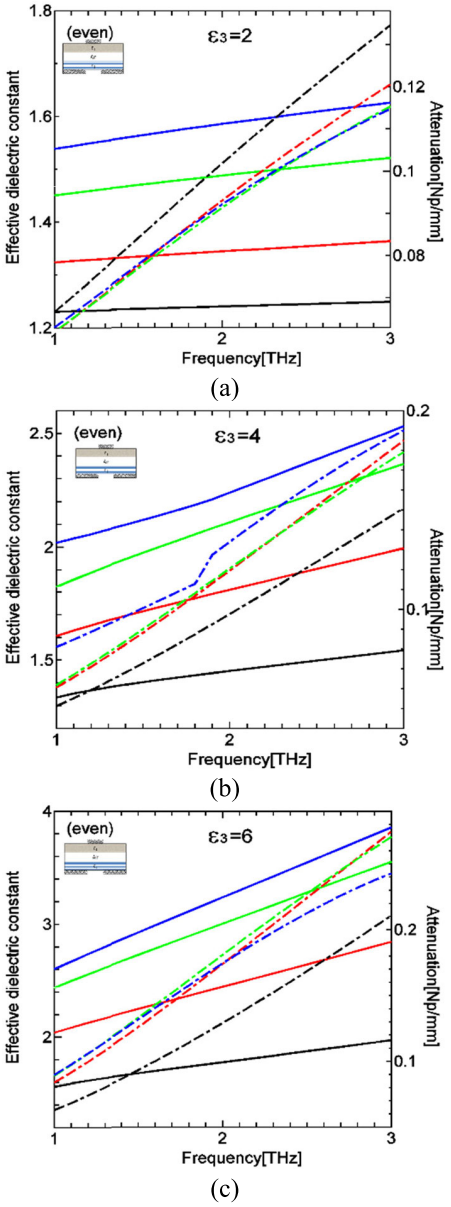

FIGURE 17. Under even mode excitation, the effective dielectric constant versus frequency curves when ε_3 is (a) 2, (b) 4, (c) 6. Solid lines represent effective dielectric constant, dotted lines represent attenuation.

attenuation constant decreases, i.e., the radiation loss decreases dramatically, significantly affecting the change of the attenuation constant, and the attenuation constant is down-regulated.

In another case, the thickness of the first layer of dielectric substrate, fixed to 4um, remains unchanged, and the same material with the dielectric constant of 2 is ensured. The thickness and dielectric constant of the third layer of dielectric substrate are changed, and the transmission characteristics are measured and compared under different conditions.

The curves of effective dielectric constant under odd mode excitation are shown by solid line in Fig. 16. When the dielectric constant of the third layer is 2, 4, and 6, respectively, the effective dielectric constant is simulated, suggesting no difference between the effective dielectric constant of the third layer substrate and that of the first layer substrate. The larger the thickness, the bigger the effective dielectric constant will be.

The attenuation curve of three-layer dielectric structure under odd mode excitation is shown in Fig. 16. The general trend is that the attenuation changes with the rise in dielectric constant of the third layer dielectric substrate. With the change of thickness, the effect of attenuation varies. The larger the thickness, the larger the conductor loss will be, whereas with the rise in dielectric constant, the dielectric loss will increase. When the dielectric constant reaches 6, the radiation loss decreases noticeably, and the corresponding attenuation begins to decrease.

The effective dielectric constant of the structure under even mode excitation is analyzed. As shown by solid line in Fig. 17, the effective dielectric constant increases with the rise in the dielectric constant of the third layer dielectric substrate. Likewise, under the same dielectric condition, the effective dielectric constant increases with the rise in the thickness of the third layer dielectric substrate.

The attenuation constant curve of three-layer dielectric structure under dual mode excitation is shown by dotted line in Fig. 17. When the dielectric constant of the third layer is 2, it is found that when the thickness is 4×10^{-3}mm, the attenuation value is obviously greater than that under other thickness values. Moreover, with the rise in the thickness, the attenuation curve almost coincides. When the dielectric constant of the third layer substrate is 4, the attenuation value will be the maximum at the thickness of 14×10^{-3}mm, while the attenuation value will be the minimum at the thickness of 4×10^{-3}mm. When the dielectric constant of the third layer is 6 and the thickness is 4×10^{-3}mm, the attenuation is the smallest. With the rise in the thickness, the attenuation curve will almost coincide, whereas the attenuation decreases when the thickness reaches 14×10^{-3}mm.

IV. COMPARSION OF ATTENUATION CONSTANTS OF THREE-LAYER, DOUBLE-LAYER AND SINGLE-LAYER STRUCTURES

By comparing the lowest loss structure of the two-layer medium and the three-layer medium discussed above with the single-layer medium structure, better transmission characteristics [43] can be achieved. The experimental data are obtained, and the minimum attenuation is obtained by changing the dielectric constant of the single-layer structure substrate. Subsequently, in the three structures mentioned in this paper, the data required are taken to draw a comparison of attenuation and effective dielectric constant.

Fig. 18 refers to a parametric comparison diagram of microstrip-slot coupling structures of single-layer, double-layer and three-layer dielectrics excited in even and odd modes. The solid lines represent effective dielectric constant. The dotted lines represent attenuation. The black lines represent the single layer dielectric structures with dielectric constants of 2. One red line represents the double-layer

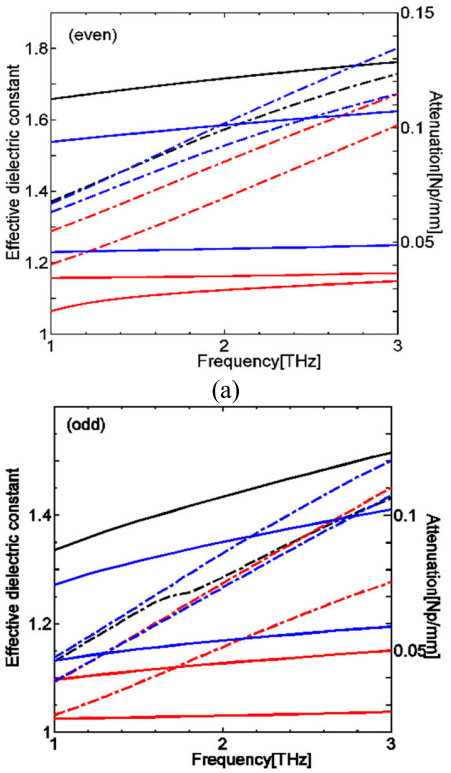

FIGURE 18. Comparison of attenuation constants under even mode excitation (a) and odd mode excitation (b). Solid lines represent effective dielectric constant, dotted lines represent attenuation.

dielectric structure with upper layer's dielectric constant ε_1 of 2 and thickness d1 of 4 um in the upper layer. The other red line represents the double-layer dielectric structure with lower layer's dielectric constant ε_3 of 2 and thickness d2 of 4×10^{-3}mm in the lower layer. The blue line represents the three-layer structure when $\varepsilon_1 = 2$, d1 $= 4 \times 10^{-3}$mm, $\varepsilon_3 = 2$, d3 $= 14 \times 10^{-3}$mm. The other blue line represents the three-layer structure when $\varepsilon_1 = 2$, d1 $= 4 \times 10^{-3}$mm, $\varepsilon_3 = 2$, d3 $= 4 \times 10^{-3}$mm.

Fig. 18 suggests that the lowest losses in all cases discussed in the previous section are not lower than those in double-layer dielectric structures, whereas they are lower than those in single-layer dielectric structures under even-mode excitation. In the case of odd mode excitation, when $\varepsilon_1 = 2$, d1 $= 4 \times 10^{-3}$mm, $\varepsilon_3 = 2$, d3 $= 4 \times 10^{-3}$mm, the loss of three-layer dielectric structure will be lower than that of single-layer dielectric structure. The results of the graph analysis indicate that when $\varepsilon_1 = 2$, d1 $= 4 \times 10^{-3}$mm, $\varepsilon_3 = 2$, d3 $= 4 \times 10^{-3}$mm, three-layer microstrip-slot coupling structure with air in the middle will exhibit better transmission characteristics.

V. CONCLUSION

In the present paper, the transmission characteristics of the double-layer micro-strip-slot coupling structure with air in the upper layer and the double-layer microstrip-slot coupling structure with air in the lower layer in terahertz band are investigated. When frequency is above 1 THz, the effective dielectric constant and attenuation constant of two types of double-layer substrates are similar. In comparison, the attenuation constant under even mode excitation is smaller than that under odd mode excitation. The proportions of air to substrate also significantly affects the transmission characteristics. In the meantime, the three-layer structure is also studied, an air layer is placed between the two-layer transmission substrates, and the transmission characteristics of the two-layer dielectric substrates are compared with the dielectric constant and the thickness of the dielectric substrates as variables. It is found that the thickness and dielectric constant of the substrate significantly affect the attenuation. The variation of effective dielectric constant is almost the same. With the rise in dielectric constant and thickness, the dielectric constant of the transmission dielectric plate is changed to a certain extent by the existence of air layer, while the overall conductor loss, dielectric loss and radiation loss are changed as well. From the discussion of single-layer structure, double-layer structure and three-layer structure, it is suggested that the attenuation constants of double-layer medium and three-layer medium are nearly the identical, whereas the attenuation of the structure with air layer is noticeably smaller than that of single-layer structure.

REFERENCES

[1] K. R. Jha and G. Singh, "Analysis of narrow terahertz microstrip transmission-line on multilayered substrate," *J. Comput. Electron.*, vol. 10, pp. 186–194, Jun. 2011.

[2] J. Federici and L. Moeller, "Review of terahertz and sub-terahertz wireless communications," *Appl. Phys. Lett*, vol. 107, no. 11, 2010, Art. no. 111101.

[3] J. Dai, B. Clough, I-C. Ho, X. Lu, J. Liu, and X.-C. Zhang , "Recent progresses in terahertz wave air photonics," *IEEE Trans. THz Sci. Technol.*, vol. 1, no. 1, pp. 274–281, Sep. 2011.

[4] A. G. Markelz, A. Roitberg, and E. Heilweil, "Pulsed terahertz spectroscopy of DNA, bovine serum albumin and collagen between 0.1 and 2.0 THz," *Chem. Phys. Lett*, vol. 320, nos. 1–2, pp. 42–48, Mar. 2000.

[5] A. Cavalleri, S. Wall, and C. S. Pson, "Tracking the motion of charges in a terahertz light field by femtosecond X-Ray diffraction," *Nature*, vol. 442, no. 7103, pp. 664–666, 2006.

[6] M. C. Kemp, P. F. Taday, B. E. Cole, J. A. Cluff, A. J. Fitzgerald, and W. R. Tribe, "Security applications of terahertz technology," *Proc. SPIE, THz Mil. Secur. Appl.*, vol. 5070, pp. 44–52, Aug. 2003.

[7] J. Wang, Y. Ding, S. Bian, Y. Peng, M. Liu, and G. Gui, "UL-CSI data driven deep learning for predicting DL-CSI in cellular FDD systems," *IEEE Access*, vol. 7, pp. 96105–96112, 2019.

[8] G. Gui, H. Huang, Y. Song, and H. Sari, "Deep learning for an effective nonorthogonal multiple access scheme," *IEEE Trans. Veh. Technol.*, vol. 67, no. 9, pp. 8440–8450, Sept. 2018.

[9] Y. Wang, M. Liu, J. Yang, and G. Gui, "Data driven deep learning for automatic modulation recognition in cognitive radios," *IEEE Trans. Veh. Technol.*, vol. 68, no. 4, pp. 4074–4077, Apr. 2019.

[10] J. A. Harrington, R. George, P. Pedersen, and E. Mueller, "Hollow polycarbonate waveguides with inner Cu coatings for delivery of terahertz radiation," *Opt. Express*, vol. 12, no. 21, pp. 5263–5268, 2004.

[11] B. Bowden, J. A. Harrington, and O. Mitrofanov, "Silver/polystyrene-coated hollow glass waveguides for the transmission of terahertz radiation," *Opt. Lett*, vol. 32, no. 20, pp. 2945–2947, 2007.

[12] B. Bowden, J. A. Harrington, and O. Mitrofanov, "Fabrication of terahertz hollow-glass metallic waveguides with inner dielectric coatings," *App. Phys. Lett*, vol. 104, 2008, Art. no. 093110.

[13] S. D. Wu, A. Argyros, and G. S. Leon-Saval, "Reducing the size of hollow terahertz waveguides," *J. Lightw. Technol.*, vol. 29, no. 1, pp. 93–103, 2011.

[14] R. Mendis. *First Broadband Experimental Study of Planar THz Wave-Guides*. Stillwater, OK, USA: Oklahoma State Univ., 2001.
[15] R. Mendis and D. Grischkowsky, "Undistorted guided-wave propagation of subpicosecond terahertz pulses," *Opt. Lett.*, vol. 26, no. 11, pp. 846–848, 2001.
[16] K. Wang and D. M. Mittleman, "Metal wires for terahertz wave guiding," *Nature*, vol. 432, no. 7015, pp. 376–379, 2004.
[17] M. King and J. C. Wiltse, "Surface-wave propagation on coated or uncoated metal wires at millimeter wavelengths," *IRE Trans. Antennas Propag.*, vol. AP-10, no. 3, pp. 246–254, May 1962.
[18] K. C. Gupta, R. Garg, I. Bahl, and P. Bhartia, *Microstrip Lines and Slotlines*, 2nd ed. Norwood, MA, USA: Artech House, 1996.
[19] R. K. Hoffmann and J. Siegl, "Microstrip-slot coupler design—Part I: S-parameters of uncompensated and compensated couplers," *IEEE Trans. Microw. Theory Techn.*, vol. MTT-30, no. 8, pp. 1205–1210, Aug. 1982.
[20] R. K. Hoffmann and J. Siegl, "Microstrip-slot coupler design—Part II: Practical design aspects," *IEEE Trans. Microw. Theory Techn.*, vol. MTT-30, no. 8, pp. 1211–1216, Aug. 1982.
[21] Y. Liu, S. Li, S. Zhu, and X. Lv, "New two-dimensional PBG structures for THz transmission line and antenna integrated design based on MEMS technology," in *Proc. Int. Conf. Microw. Millim. Wave Technol. (ICMMT)*, Chengdu, China, May 2010, pp. 1683–1686.
[22] Y. Kadoya, "THz wave propagation on strip lines: Devices, properties, and applications," in *Proc. 19th Int. Conf. Appl. Electromagn. Commun.*, Jun. 2008.
[23] S. Atakaramians, A. Argyros, S. C. Fleming, and B. T. Kuhlmey, "Hollow-core waveguides with uniaxial metamaterial cladding: Modal equations and guidance conditions," *J. Opt. Soc. Amer. B, Opt. Phys.*, vol. 29, no. 9, pp. 2462–2477, Sep. 2012.
[24] K. Geim and K. S. Novoselov, "The rise of grapheme," *Nature Mater.*, vol. 6, pp. 183–191, 2007.
[25] V. P. Gusynin, S. G. Sharapov, and J. P. Carbotte, "Magneto-optical conductivity in graphene," *J. Phys., Condens. Matter*, vol. 19, no. 2, Jun. 2006, Art. no. 026222.
[26] Z. Wang, Y. Zhang, R. Xu, and W. Lin, "Investigation of THz Sommerfeld wave propagation on single-wire at different temperature," *Optik*, vol. 123, pp. 2159–2165, 2012.
[27] M. Wächter, M. Nagel, and H. Kurz, "Metallic slit waveguide for dispersion-free low-loss terahertz signal transmission," *Appl. Phys. Lett.*, vol. 90, Jan. 2007, Art. no. 061111.
[28] N. Mora, G. Lugrin, F. Rachidi, I. Junqua, J. P. Parmantier, S. Tkachenko, M. Rubinstein, M. Nyffeler, and P. Bertholet, "On the validity limits of the transmission line theory in evaluating differential-mode signals along a two-wire line above a ground plane," in *Proc. IEEE Int. Symp. Electromagn. Compat. (EMC)*, Aug. 2015, pp. 797–800.
[29] F. C. de Ronde, "A new class of microstrip directional couplers," in *Proc. G-MTT Int. Microw. Symp.*, May 1970, pp. 184–189.
[30] R. A. Pucel, D. J. Massé, and C. P. Hartwig, "Losses in microstrip," *IEEE Trans. Microw. Theory Techn.*, vol. MTT-16, no. 6, pp. 342–350, Jun. 1968.
[31] B. R. Rao, "Effect of loss and frequency dispersion on the performance of microstrip directional couplers and coupled line filters (short papers)," *IEEE Trans. Microw. Theory Techn.*, vol. MTT-22, no. 7, pp. 747–750, Jul. 1974.
[32] S. B. Cohn, "Slot line on a dielectric substrate," *IEEE Trans. Microw. Theory Techn.*, vol. MTT-17, no. 10, pp. 768–778, Oct. 1969.
[33] D. Gacemi, A. Degiron, M. Baillergeau, and J. Mangeney, "Identification of several propagation regimes for terahertz surface waves guided by planar Goubau lines," *Appl. Phys. Lett.*, vol. 103, no. 19, 2013, Art. no. 191117.
[34] T. Chen, S. Junqiang, L. Li, J. Tang, and Y. Zhou, "Design of a photonic crystal waveguide for Terahertz-wave difference-frequency generation," *IEEE Photon. Technol. Lett*, vol. 24, no. 11, pp. 921–923, Jun. 1, 2012.
[35] M. Stecher, C. Jansen, M. Ahmadi-Boroujeni, R. Lwin, A. Stefani, M. Koch, and G. Town, "Polymeric THz 2D photonic crystal filters fabricated by fiber drawing," *IEEE Trans. THz Sci. Technol*, vol. 2, no. 2, pp. 203–207, Mar. 2012.
[36] T. Tanaka, K. Tsunoda, and M. Aikawa, "Slot-coupled directional couplers between double-sided substrate microstrip lines and their applications," *IEEE Trans. Microw. Theory Techn.*, vol. MTT-36, no. 12, pp. 1752–1757, Dec. 1988.
[37] M. Aikawa and H. Ogana, "Double-sided MICs and their applications," *IEEE Trans. Microw. Theory Techn.*, vol. MTT-37, no. 2, pp. 406–413, Feb. 1989.
[38] R. N. Simons, N. I. Dib, and L. P. B. Katehi, "Modeling of coplanar stripline discontinuities," *IEEE Trans. Microw. Theory Techn.*, vol. 44, no. 5, pp. 711–716, May 1996.
[39] G. Duchamp, L. Casadebaig, S. Gauffre, and J. Pistre, "An alternative method for end-effect characterization in shorted slotlines," *IEEE Trans. Microw. Theory Techn.*, vol. 46, no. 11, pp. 1793–1795, Nov. 1998.
[40] M. Matsunaga, M. Katayama, and K. Yasumoto, "Coupled-mode analysis of line parameters of coupled microstrip lines," *Prog. Electromagnetices Res.*, vol. 24, pp. 1–17, 1999.
[41] K. Yasumoto, "Coupled-mode formulation of multilayered and multiconductor transmission lines," *IEEE Trans. Microw. Theory Tech.*, vol. MTT-44, no. 4, pp. 585–590, Apr. 1996.
[42] K. Yasumoto and M. Matsunaga, "Coupled-mode analysis of coupled multiple microstrip lines," *IEICE Trans. Electron.*, vols. E80–C, pp. 340–345, Feb. 1997.
[43] T. Itoh, *Numerical Techniques for Microwave and Millimeter Wave Passive Structures*. New York, NY, USA: Wiley, 1989.
[44] J. Zhu and D. Zhang, "Terahertz wave propagation characteristics of multi-modes on complexity microstrip-slot coupled lines," *IEICE Electron. Exp.*, vol. 15, no. 16, pp. 1–6, 2018.
[45] M. Y. Frankel, S. Gupta, J. A. Valdmanis, and G. A. Mourou, "Terahertz attenuation and dispersion characteristics of coplanar transmission lines," *IEEE Trans. Microw. Theory Techn.*, vol. 39, no. 6, pp. 910–916, Jun. 1991.
[46] A. Tsuchiya and H. Onodera, "Impact of radiation loss in on-chip transmission-line for Terahertz applications," in *Proc. 16th IEEE Workshop Signal Power Integrity (SPI)*, May 2012, pp. 125–128.

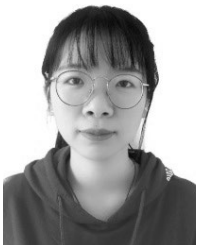

XINYU WANG was born in Nantong, China, in 1996. She received the B.S. degree in electronic information engineering from the College of Information Science and Technology, Nanjing Forestry University, Nanjing, China, in 2018, where she is currently pursuing the M.S. degree in instrument and meter engineering. Her current interest includes multilayer structures in terahertz bands.

DAN ZHANG (M'09) received the B.S. degree in mechanical engineering from the Dalian University of Technology, Dalian, China, in 1999, and the M.S. and Ph.D. degrees in electromagnetic waves and communication engineering from Kyushu University, Fukuoka, Japan, in 2004 and 2007, respectively. He is currently a Professor of electronic and communication engineering with the College of Information Science and Technology, Nanjing Forestry University, China. In 2015, he was introduced to Nanjing Forestry University as a high-level talent. In recent years, more than 50 articles have been published by the first author, and more than ten patents have been applied for granted. His research has been focused on electromagnetic field theory, microwave and optical technology, and nondestructive testing and imaging. He has been invited by the International Professional Society for many times to preside over international conferences or give academic speeches. He is currently an Associate Editor of *IEICE Electronics Express*, and a Reviewer of several internationally renowned professional journals.

JING ZHU was born in Yangzhou, China, in 1994. She received the B.S. degree in electronic information engineering and the M.S. degree in precision instruments and machinery from the College of Information Science and Technology, Nanjing Forestry University, Nanjing, China, in 2016 and 2019, respectively. She is currently engaged in the research of microwave devices.